New Journal of Physics
The open access journal at the forefront of physics

Deutsche Physikalische Gesellschaft DPG IOP Institute of Physics

Spin filtering induced by a magnetic insulator stripe on graphene

New Journal of Physics
The open access journal at the forefront of physics

Deutsche Physikalische Gesellschaft DPG
IOP Institute of Physics

Published in partnership with: Deutsche Physikalische Gesellschaft and the Institute of Physics

OPEN ACCESS

RECEIVED
26 January 2021

REVISED
22 April 2021

ACCEPTED FOR PUBLICATION
29 April 2021

PUBLISHED
20 May 2021

PAPER

Spin filtering induced by a magnetic insulator stripe on graphene

C H Fuentevilla[1,*], J D Lejarreta[1], F Domínguez-Adame[2] and E Diez[1]

[1] Group of Nanotechnology, USAL-NANOLAB, Universidad de Salamanca, E-37008 Salamanca, Spain
[2] GISC, Departamento de Física de Materiales, Universidad Complutense, E-28040 Madrid, Spain
* Author to whom any correspondence should be addressed.

E-mail: chernan@usal.es

Keywords: graphene, ferromagnetic insulator, ferrimagnetic insulator, spintronics, 2D materials

Abstract

Proximity exchange interaction between graphene electrons and nearby magnetic insulators paves the way to create spin-polarised currents for spintronics applications. Different ferro- and ferrimagnetic insulators, such as europium chalcogenides, yttrium iron garnet and cobalt ferrite, have been proposed in the literature to induce magnetic correlations in graphene. We theoretically study electronic transport properties of graphene in close proximity to a strip of a magnetic insulator, when the system is connected to nonmagnetic source and drain leads. To this end, we describe graphene electrons by means of an effective Hamiltonian whose model parameters are extracted from first-principle calculations. We compare the spin-polarization of the electron current calculated for a number of different magnetic insulators, aiming at elucidating the effects of the various model parameters on the efficiency of the device. In particular, we demonstrate that the polarization of the electric current across the device can be tuned by the source–drain voltage. We conclude that the heterostructures based on europium chalcogenides are ideal candidates to achieve high polarisation at low temperature.

1. Introduction

Graphene is oftenly envisioned as a promising candidate to supersede semiconductors as the basic material for the design of innovative nanodevices. The truly two-dimensional geometry as well as large carrier mobility (over two order of magnitudes larger than silicon) make graphene suitable for a wide range of applications in electronics [1]. In this context, spin-based electronics (spintronics) exploits the electron spin degree of freedom [2] and put forward new ways for efficient and reliable manipulation and storage of data. Therefore, spin-related and magnetic effects in graphene have been the focus of special interest for their relevance in spintronics [3–7]. In particular, ferromagnetic insulators such as europium chalcogenides (EuO and EuS, displaying giant proximity magnetoresistance [8]) deposited on graphene can induce ferromagnetic correlations [9]. For instance, epitaxial growth of EuO onto graphene was reported in reference [10] and magneto-optic measurements indicate that the Curie temperature of thin films reaches the value of bulk EuO (∼69 K). Due to the proximity exchange interaction between magnetic ions and graphene electrons, nanostructures such as tunnel barriers [9, 11], quantum rings [12–14] and superlattices [15] can operate as spin filters and sustain spin-dependent Bloch oscillations.

As a first approximation, the proximity exchange interaction can be viewed as an effective Zeeman splitting of the spin sublevels [9, 16, 17]. The interaction has the characteristic length scale of one atomic layer. Therefore, the splitting is induced only in the regions of graphene which are in close contact to the ferromagnetic insulator. As a consequence, electrons propagating along the sample will be subjected to a spin-dependent potential, leading to spin-polarized currents. However, detailed *ab initio* calculations demonstrate that the scenario is more intricate [18, 19]. According to density functional theory simulations, the parameters of the effective electron Hamiltonian around the K and K' valleys of graphene in close proximity to a narrow film of a ferromagnetic or ferrimagnetic insulator (FMI) depend on the layer

Table 1. Material-dependent parameters of the graphene/FMIs structures used in our calculations, retrieved from references [8, 17, 19–21]. EuO/Gr/EuO aligned and misaligned structures differ by the alignment of the EuO monolayer on opposite sides of the graphene layer [20].

Structure	δ (meV)	Δ (meV)	m (meV)	$v_\uparrow/v_F$	$v_\downarrow/v_F$
EuO/Gr/EuO(1BL) aligned	199.5	326.5	−17.5	1.34	1.63
EuO/Gr/EuO(1BL) misaligned	215.5	159.5	−4.5	1.34	1.63
Gr/EuO(6BL)	66.0	116.0	18.0	1.34	1.63
Gr/EuS(6BL)	6.5	175.0	16.6	1.40	1.70
$Gr/Y_3Fe_5O_{12}$	−83.5	84.0	31.5	0.54	0.60
$Gr/CoFe_3O_4$	−47.0	10.0	2.0	0.21	0.23

thickness. Furthermore, in addition to the aforementioned exchange coupling induced by the magnetic ions, the fact that the graphene sublattices feel different potential might result in a spin-dependent gap opening at the Dirac point [19]. Finally, a spin-dependent mass term in the effective electron Hamiltonian is needed to reproduce the band structure obtained by first-principle calculations. The combination of all these interactions have an impact on the spin-filtering capabilities of the device that remains rather unexplored. The aim of this work is to present a thorough study of the effects of the various interaction terms that arise in a realistic description of graphene electrons in close proximity to a strip of a ferromagnetic insulator (EuO and EuS) or a FMI (yttrium iron garnet, YIG, and cobalt ferrite, CFO). The spin-polarization of the electron current when the system is connected to nonmagnetic source and drain leads will be used as a figure of merit for the assessment of the device. The combination of the exchange splitting due to the interaction of the electron spin with the magnetic ions and the effect of the source–drain voltage can result in a controllable spin-polarized electric current. Most importantly, we have found that the highest value of the current density polarization at low temperature is reached with EuO/Gr/EuO heterostructures.

2. Model and effective Hamiltonian

We investigate spin-dependent electron transport through a hybrid nanostructure formed by a strip of a ferro- or FMI grown on top (or top and below, see table 1) of bulk graphene. The hybrid system is connected to nonmagnetic source and drain leads, as sketched in figure 1(a). A gate voltage creates a potential energy barrier of height U_0 for electrons in the region of graphene which is in close proximity to the FMI. The electric potential profile due to the presence of the gate voltage can be calculated by solving the Poisson and Schrödinger equations self-consistently. However, for simplicity, we assume a square potential profile, as shown in figure 1(b). We address the current and its polarization at a finite bias voltage between source (S) and drain (D), whose chemical potentials, $\mu_S = \mu$ and $\mu_D = \mu - eV_{SD}$, have the same offset μ from the Dirac point. For concreteness, we restrict ourselves to the case $\mu = 0$ in our calculations.

The Hamiltonian describing the electron dynamics in pristine graphene is given as

$$H_0 = \hbar v_F \mathbb{1}_s \otimes \boldsymbol{\sigma} \cdot \boldsymbol{k}, \tag{1a}$$

where $\hbar v_F = 658$ meV nm. In the graphene region in close proximity to the FMI stripe ($a < x < a + L$), the proximity exchange interaction leads to the following electron Hamiltonian [19]

$$H_{FMI} = \hbar \mathbb{v}_s \otimes \boldsymbol{\sigma} \cdot \boldsymbol{k} + \frac{\delta}{2} s_z \otimes \mathbb{1}_\sigma + \frac{\Delta}{2} \mathbb{1}_s \otimes \sigma_z + \frac{m}{2} s_z \otimes \sigma_z + U_0 \mathbb{1}_s \otimes \mathbb{1}_\sigma, \tag{1b}$$

with

$$\mathbb{v}_s = \begin{pmatrix} v_\uparrow & 0 \\ 0 & v_\downarrow \end{pmatrix}, \tag{1c}$$

where the matrix $\mathbb{v}_s$ acts on spin space. $\mathbb{1}_\sigma$ is the identity matrix and σ_x, σ_y and σ_z are the corresponding Pauli matrices, acting on pseudospin space (sublattices A and B of graphene). Similarly, $\mathbb{1}_s$ and s_z are the identity and a Pauli matrix acting on spin space, and the symbol $\otimes$ stands for the Kronecker product. The proximity exchange splitting of the electronic states is accounted for by the first term of H_{FMI}. The second term takes into account that both graphene sublattices feel different potential and the third term is a spin-dependent gap [19]. Notice that intervalley scattering opens up a trivial gap [20] but its magnitude is small and it will be neglected in the present analysis. Parameters used in our calculations are listed in table 1.

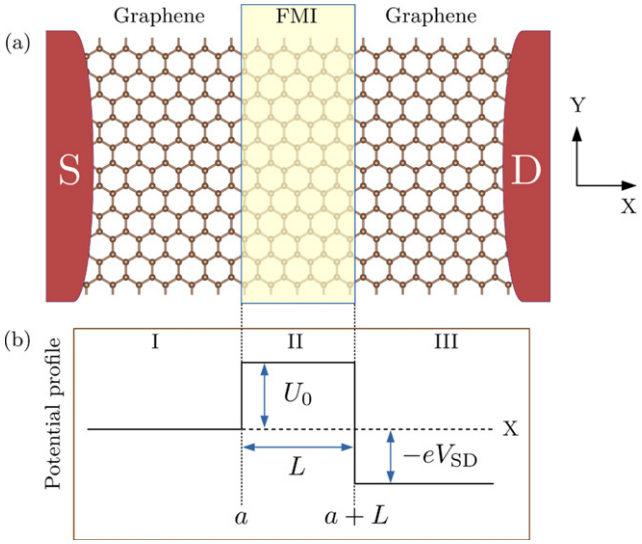

Figure 1. (a) Sketch of the spintronic device. A strip of a ferro- or ferrimagnetic insulator (FMI) is grown of top (or top and below, see table 1) of bulk graphene and the device is then connected to source (S) and drain (D) leads. (b) A gate voltage creates an additional potential energy barrier of height U_0 for electrons in the region of graphene which are in close proximity to the FMI. For simplicity, the potential profile due to the gate voltage is assumed to be zero in regions I and III and constant in region II. The device is assumed infinite along the transverse direction Y.

The Hamiltonian $H = [1 - F(x)]H_0 + F(x)H_{\rm FMI}$ acts upon the four-component wave function $\mathbf{\Psi}(x, y)$ corresponding to the sublattice (A and B) and spin ($\uparrow$ and $\downarrow$) degrees of freedom. Here $F(x) = 1$ for $a < x < a + L$ and vanishes otherwise (the proximity exchange interaction appears only when the graphene electron is located in region II shown in figure 1). The four-component wave function can be cast in a more compact form as

$$\mathbf{\Psi}(x,y) = \begin{pmatrix} \psi_\uparrow(x,y) \\ \psi_\downarrow(x,y) \end{pmatrix} = \begin{pmatrix} A_\uparrow(x,y) \\ B_\uparrow(x,y) \\ A_\downarrow(x,y) \\ B_\downarrow(x,y) \end{pmatrix}. \tag{2a}$$

Hence $H\mathbf{\Psi}(x, y) = E\mathbf{\Psi}(x, y)$ with

$$H = \begin{pmatrix} c_1F(x) & \hbar\tilde{v}_\uparrow(x)k_- & 0 & 0 \\ \hbar\tilde{v}_\uparrow(x)k_+ & c_2F(x) & 0 & 0 \\ 0 & 0 & c_3F(x) & \hbar\tilde{v}_\downarrow(x)k_- \\ 0 & 0 & \hbar\tilde{v}_\downarrow(x)k_+ & c_4F(x) \end{pmatrix} + U_0F(x)\mathbb{1}_4, \tag{2b}$$

where $\mathbb{1}_4$ is the 4×4 unity matrix. We have also defined $k_\pm = k_x \pm \mathrm{i}k_y$, $\tilde{v}_s(x) = [1 - F(x)]v_{\rm F} + F(x)v_s$ ($s = \uparrow, \downarrow$) and the following material-dependent parameters

$$\begin{aligned} c_1 &= \frac{m}{2} + \frac{\delta}{2} + \frac{\Delta}{2}, \qquad c_2 = -\frac{m}{2} + \frac{\delta}{2} - \frac{\Delta}{2}, \\ c_3 &= -\frac{m}{2} - \frac{\delta}{2} + \frac{\Delta}{2}, \qquad c_4 = \frac{m}{2} - \frac{\delta}{2} - \frac{\Delta}{2}. \end{aligned} \tag{2c}$$

3. Energy bands of hybrid graphene/FMI structures

Before calculating the electric current through the device sketched in figure 1, it is instructive to discuss the band structure of hybrid graphene/FMI systems. In our model this can be accomplished by taking the width of the FMI strip $L \to \infty$, i.e. we replace $F(x) \to 1$ in the Hamiltonian H given in equation (2b). Spin-up and spin-down conduction and valence bands are then easily calculated by direct diagonalization of the Hamiltonian H

$$\begin{aligned} E_\uparrow(\boldsymbol{k}) &= U_0 + \frac{\delta}{2} \pm \sqrt{\frac{1}{4}(\Delta + m)^2 + \hbar^2 v_\uparrow^2 \left(k_x^2 + k_y^2\right)}, \\ E_\downarrow(\boldsymbol{k}) &= U_0 - \frac{\delta}{2} \pm \sqrt{\frac{1}{4}(\Delta - m)^2 + \hbar^2 v_\downarrow^2 \left(k_x^2 + k_y^2\right)}. \end{aligned} \tag{3}$$

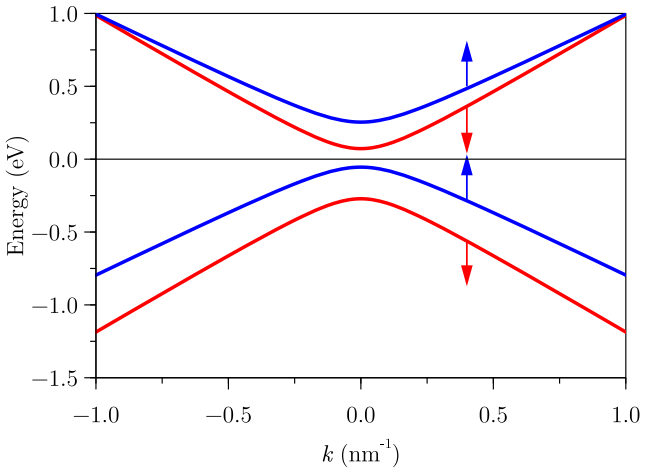

Figure 2. Calculated spin-dependent energy bands (3) for the EuO/Gr/EuO(1BL) aligned hybrid structure, using the parameters given in table 1 with $U_0 = 0$. The proximity exchange interaction of graphene electrons with the FMI splits the bands and open spin-dependent gaps. The blue and red lines indicate the bands for spin-up and spin-down states, respectively.

The proximity exchange interaction of graphene electrons with the FMI opens a sizable gap of magnitude $|\Delta + m|$ and $|\Delta - m|$ for spin-up and spin-down electrons, respectively. As an example, figure 2 shows the spin-dependent energy bands (3) for the EuO/Gr/EuO(1BL) aligned hybrid structure, calculated with the parameters given in table 1. The band structure can be shifted upwards or downwards an amount U_0 by means of a gate voltage, what is crucial to control the spin-polarized current through the device shown in figure 1.

4. Spin-polarized current

In this section we focus on the spin-polarized current through the nanodevice. Assuming that electron–phonon scattering in our samples is reduced, we consider electrons in fully coherent regime transferring ballistically through the system. We obtain the transmission coefficient as a function of energy in a device with an FMI barrier of finite width L and use the Landauer–Büttiker scattering formalism to calculate the current.

Since the system is translationally invariant in the transverse direction, the corresponding component of the wave vector is conserved. Therefore, the wave function (2a) can be factorized as follows

$$\Psi(x,y) = \mathrm{e}^{\mathrm{i}k_y y}\begin{pmatrix}\varphi_\uparrow(x)\\ \varphi_\downarrow(x)\end{pmatrix}. \tag{4}$$

In the biased nanostructure ($V_{\mathrm{SD}} \neq 0$), the longitudinal component of the wave vector in regions I and III (pristine graphene) reads

$$k_{\mathrm{I}x} = \sqrt{\left(\frac{E}{\hbar v_{\mathrm{F}}}\right)^2 - k_y^2}, \qquad k_{\mathrm{III}x} = \sqrt{\left(\frac{E+eV_{\mathrm{SD}}}{\hbar v_{\mathrm{F}}}\right)^2 - k_y^2}. \tag{5}$$

Electron states are spin-degenerate in these two regions ($j = \mathrm{I}, \mathrm{III}$)

$$\varphi_j(x) = C_j\,\mathrm{e}^{\mathrm{i}k_x x}\begin{pmatrix}1\\ \pm k_{j+}/k\end{pmatrix} + D_j\,\mathrm{e}^{-\mathrm{i}k_x x}\begin{pmatrix}1\\ \mp k_{j-}/k\end{pmatrix}, \tag{6}$$

where the upper (lower) sign refers to the conduction (valence) bands and C_j and D_j are integration constants. We defined $k_{j\pm} = k_{jx} \pm \mathrm{i}k_y$ for the sake of brevity. The proximity exchange interaction of graphene electrons with the magnetic ions in region II breaks the spin degeneracy and the wave function is

written down as follows

$$\varphi_{\uparrow,\mathrm{II}}(x) = C_{\uparrow,\mathrm{II}}\, \mathrm{e}^{\mathrm{i}q_\uparrow x}\begin{pmatrix} 1 \\ \dfrac{2\hbar v_\uparrow(q_\uparrow + \mathrm{i}k_y)}{\Delta + m \pm \rho_\uparrow}\end{pmatrix} + D_{\uparrow,\mathrm{II}}\, \mathrm{e}^{-\mathrm{i}q_\uparrow x}\begin{pmatrix} 1 \\ -\dfrac{2\hbar v_\uparrow(q_\uparrow - \mathrm{i}k_y)}{\Delta + m \pm \rho_\uparrow}\end{pmatrix},$$
$$\varphi_{\downarrow,\mathrm{II}}(x) = C_{\downarrow,\mathrm{II}}\, \mathrm{e}^{\mathrm{i}q_\downarrow x}\begin{pmatrix} 1 \\ \dfrac{2\hbar v_\downarrow(q_\downarrow + \mathrm{i}k_y)}{\Delta - m \pm \rho_\downarrow}\end{pmatrix} + D_{\downarrow,\mathrm{II}}\, \mathrm{e}^{-\mathrm{i}q_\downarrow x}\begin{pmatrix} 1 \\ -\dfrac{2\hbar v_\downarrow(q_\downarrow - \mathrm{i}k_y)}{\Delta - m \pm \rho_\downarrow}\end{pmatrix}, \tag{7}$$

for spin-up and spin-down electrons, respectively. We have the following parameters for spin-up states

$$q_\uparrow = \sqrt{\left(\frac{E - U_0 - \delta/2}{\hbar v_\uparrow}\right)^2 - \left(\frac{\Delta + m}{2\hbar v_\uparrow}\right)^2 - k_y^2},$$
$$\rho_\uparrow = |2\,(E - U_0) - \delta|. \tag{8}$$

The corresponding parameters $q_\downarrow$ and $\rho_\downarrow$ for spin-down states are obtained by replacing $v_\uparrow$ by $v_\downarrow$, m by $-m$ and δ by $-\delta$ in the above expressions.

The continuity of the wave function at the edges of region II implies that $\varphi_{\mathrm{I}}(a) = \varphi_{\mathrm{s,II}}(a)$ and $\varphi_{\mathrm{s,II}}(a + L) = \varphi_{\mathrm{III}}(a + L)$ with $s = \uparrow, \downarrow$. These conditions make it possible to relate the output coefficients C_{III} and D_{III} with the input coefficients C_{I} and D_{I} by means of the 2×2 transmission matrix as follows

$$\begin{pmatrix} C_{\mathrm{III}} \\ D_{\mathrm{III}}\end{pmatrix} = \begin{pmatrix} M_{11,\mathrm{s}}(E,\phi) & M_{12,\mathrm{s}}(E,\phi) \\ M_{21,\mathrm{s}}(E,\phi) & M_{22,\mathrm{s}}(E,\phi)\end{pmatrix}\begin{pmatrix} C_{\mathrm{I}} \\ D_{\mathrm{I}}\end{pmatrix}, \tag{9}$$

where $\phi = \arctan(k_y/k_x)$ is the angle of incidence. Direct calculation of the transmission matrix shows that, for propagating states in regions I and III, the only ones relevant for transport, the conditions $M_{22} = M_{11}^*$ and $M_{21} = M_{12}^*$ hold, and $\det(M) = (k_{\mathrm{I}x}/k_{\mathrm{III}x})(1 + eV_{\mathrm{SD}}/E)$. The transmission matrix allows us to obtain the spin-dependent transmission coefficients $\tau_{\mathrm{s}}(E,\phi)$ setting $C_{\mathrm{I}} = 1$ and $D_{\mathrm{III}} = 0$, yielding

$$\tau_{\mathrm{s}}(E,\phi) = \left|\frac{k_{\mathrm{I}x}}{k_{\mathrm{III}x}}\left(1 + e\frac{V_{\mathrm{SD}}}{E}\right)\right| |M_{22,\mathrm{s}}(E,\phi)|^{-2}. \tag{10}$$

After a lengthy but straightforward calculation we get the transmission coefficient for spin-up states of the conduction and valence bands

$$\tau_\uparrow(E,\phi) = \frac{8\hbar^2 v_\uparrow^2 s_{\mathrm{I}} s_{\mathrm{III}} k_{\mathrm{I}x} k_{\mathrm{III}x} q_\uparrow^2}{A_\uparrow(E,\phi)\sin(2Lq_\uparrow) + B_\uparrow(E,\phi)\cos(2Lq_\uparrow) + C_\uparrow(E,\phi)}, \tag{11}$$

with

$$\begin{aligned} A_\uparrow(E,\phi) &= -2e\frac{v_\uparrow}{v_{\mathrm{F}}}(\Delta + m)V_{\mathrm{SD}}k_y q_\uparrow \\ B_\uparrow(E,\phi) &= 2\frac{v_\uparrow}{v_{\mathrm{F}}}[2(E - U_0) - \delta](2E + eV_{\mathrm{SD}})k_y^2 - 4\hbar^2 v_\uparrow^2(k_y^2 + q_\uparrow^2)k_y^2 - \\ &\quad - \frac{(\Delta + m)^2 + 4\hbar^2 v_\uparrow^2 k_y^2}{\hbar^2 v_{\mathrm{F}}^2}(E + eV_{\mathrm{SD}})E \\ C_\uparrow(E,\phi) &= \frac{[2(E - U_0) - \delta]^2}{\hbar^2 v_{\mathrm{F}}^2}(E + eV_{\mathrm{SD}})E + 4\hbar^2 v_\uparrow^2(k_y^4 + s_{\mathrm{I}}s_{\mathrm{III}}k_{\mathrm{I}x}k_{\mathrm{III}x}q_\uparrow^2) - \\ &\quad - 2\frac{v_\uparrow}{v_{\mathrm{F}}}[2(E - U_0) - \delta](2E + eV_{\mathrm{SD}})k_y^2, \end{aligned} \tag{12}$$

where $s_{\mathrm{I}} = \mathrm{sgn}(E)$ and $s_{\mathrm{III}} = \mathrm{sgn}(E + eV_{\mathrm{SD}})$. The corresponding transmission coefficient for spin-down states, $\tau_\downarrow(E,\phi)$, is obtained by replacing m by $-m$, $v_\uparrow$ by $v_\downarrow$, $q_\uparrow$ by $q_\downarrow$ and $\rho_\uparrow$ by $\rho_\downarrow$ in the above expressions.

Finally, following the Büttiker–Landauer method [22–24], the spin-dependent current density is obtained as follows

$$j_{x,s} = -\frac{2e}{h^2 v_{\mathrm{F}}}\int_{-\infty}^{\infty}\int_{-\pi/2}^{\pi/2}\left[f_0(E,\mu_{\mathrm{S}}) - f_0(E,\mu_{\mathrm{D}})\right]\tau_{\mathrm{s}}(E,\phi)E\,\cos\,\phi\,\mathrm{d}E\,\mathrm{d}\phi, \tag{13}$$

where f_0 stands for the Fermi–Dirac distribution function of the contacts. At low and moderate temperature we can approximate $f_0(E,\ \mu_\alpha) \approx \theta(-E,\ \mu_\alpha)$, θ being the Heaviside step function and

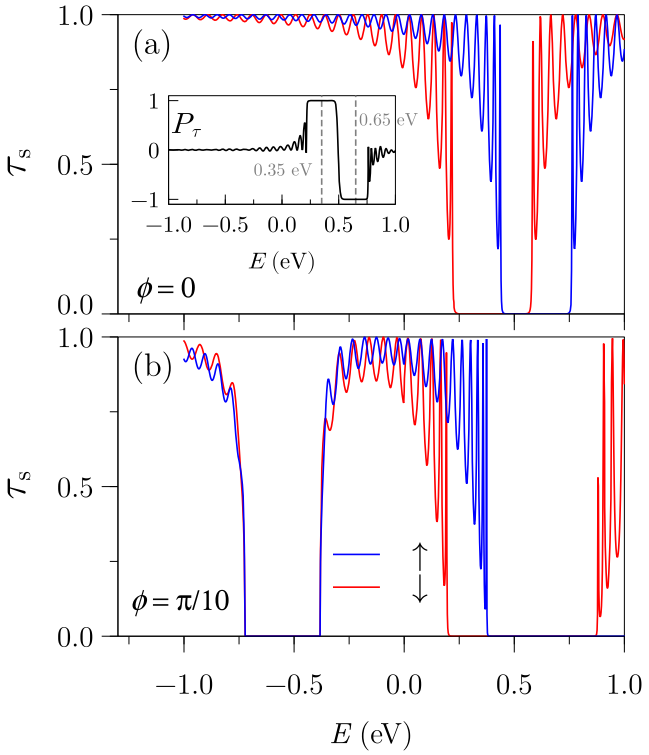

Figure 3. Spin-dependent transmission coefficient as a function of the graphene electron energy for $U_0 = 500$ meV, $V_{SD} = 0.5$ V, $L = 50$ nm and two different angles of incidence (a) $\phi = 0$ and (b) $\phi = \pi/10$ in the EuO/Gr/EuO(1BL) aligned nanostructure. Blue and red lines correspond to spin-up and spin-down states, respectively. The inset shows the transmission polarization P_τ as a function of energy at normal incidence, obtained from the data shown in panel (a).

$\alpha = \mathrm{S},\ \mathrm{D}$. Therefore

$$j_{x,s} = -\frac{2e}{h^2 v_F}\int_{\mu_S}^{\mu_D}\int_{-\pi/2}^{\pi/2}\tau_s(E,\phi)E\,\cos\,\phi\,\mathrm{d}E\,\mathrm{d}\phi\ . \tag{14}$$

We have checked that the current density calculated from equations (13) and (14) are essentially the same even at room temperature. Hence, in the next section we will calculate the current density by using (13) and (14) with $\mu_S = 0$ and $\mu_D = -eV_{SD}$.

5. Results

The sample that we address to show the capabilities of the proposed device as a spin-filter is the EuO/Gr/EuO(1BL) aligned nanostructure with a width $L = 50$ nm and a gate voltage such that $U_0 = 500$ meV. Other materials show similar trends and the comparison between them will be discussed at the end of the section. In figure 3 we show the transmission coefficient as a function of the graphene electron energy for two different angles of incidence when $V_{SD} = 0.5$ V. A spin-dependent stop-band is clearly revealed in the transmission spectrum at normal incidence (see figure 3(a)), in agreement with the band structure presented in figure 2. The stop-band can be shifted upwards or downwards in energy by changing U_0, enabling tunability of the device. The inset shows the transmission polarization, defined as $P_\tau \equiv (\tau_\uparrow - \tau_\downarrow)/(\tau_\uparrow + \tau_\downarrow)$, as a function of energy at normal incidence. We observe that full polarization is achieved over two wide energy windows centred at 0.35 eV (spin-up electrons) and 0.65 eV (spin-down electrons), respectively. Figure 3(b) displays the transmission spectrum at an incidence angle $\phi = \pi/10$. In this case, a spin-independent stop-band appears at lower energy, centred at about -0.55 eV. The origin of this spin-independent stop-band is not related to the EuO layer but to the oblique incidence of carriers considered in figure 3(b) ($\phi = \pi/10$) that breaks the usual Klein tunneling found at normal incidence ($\phi = 0$) [25, 26]. However, the two stop-bands widen upon increasing the angle of incidence but they never overlap. We have also found that the main stop-band is quite robust against variations of the incidence angle, ϕ, the width of the FMI barrier, L, and the source–drain voltage, V_{SD}. This implies that the polarization shown in the inset of figure 3(a) will determine to a large extend the current density, thus allowing the device to operate as a tunable source of polarized electrons. Below we will discuss the polarization of the current density.

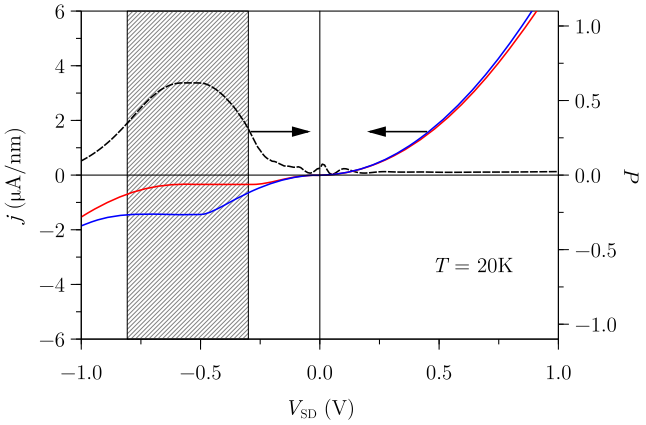

Figure 4. Current density as a function of the applied voltage between source and drain contacts for $U_0 = 500$ meV, $L = 50$ nm and $T = 20$ K in the EuO/Gr/EuO(1BL) aligned nanostructure (left axis). Blue and red solid lines correspond to spin-up and spin-down electrons, respectively. Dashed black line corresponds to the current density polarization P (right axis). Shaded area shows the voltage range of high polarisation of the current density.

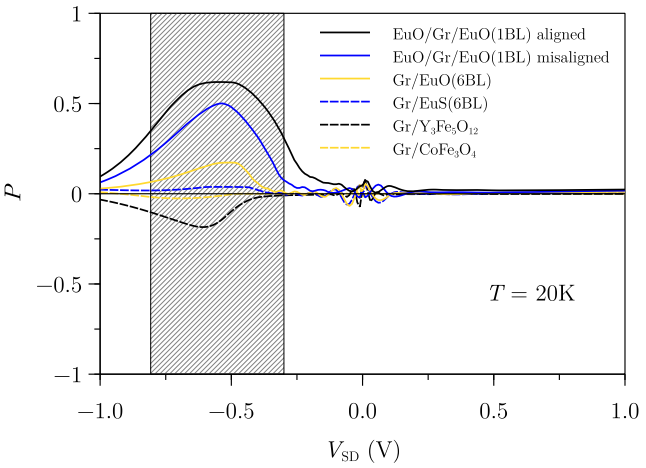

Figure 5. Current density polarisation P as a function of the source–drain voltage V_{SD} for different FMI of table 1. The parameters U_0, L and T are the same as in figure 4. Shaded area shows the voltage range of high polarisation of the current density.

The polarization of the current density is defined as

$$P = \frac{j_{x,\uparrow} - j_{x,\downarrow}}{j_{x,\uparrow} + j_{x,\downarrow}}, \tag{15}$$

and it will be the figure of merit to assess the spin-filtering properties of the device. Figure 4 displays the current density of spin-up and spin-down electrons as well as the polarization of the current density as a function of the applied voltage between the source and the drain contacts in the EuO/Gr/EuO(1BL) aligned nanostructure. We observe the appearance of high spin-polarization of the current density over a broad range at negative values of V_{SD} (shaded area in figure 4), where $P \sim 50\%$. It is most important to remark that the plateau of high polarization occurs at relatively high source–drain voltage and consequently the current density is not small. It is feasible to enhance the polarization up to perfect efficiency (100%) but usually this happens at very low source–drain voltage V_{SD} and low values of U_0 (e.g. $U_0 = 100$ meV). Hence the current density is vanishingly small, which makes it impractical for applications. In other words, one needs to seek for a balance between high efficiency and not too low current density.

Finally, we have studied the current density polarization for when the FMI stripe is fabricated with the materials listed in table 1, for the same parameters as in figure 4. The results are collected in figure 5. It becomes apparent that the highest polarization is achieved with EuO/Gr/EuO heterostructures, with $P \sim 50\%$ over a broad range of voltages. Other hybrid structures shows much lower values of the polarization of the current density for the same set of parameters.

6. Conclusions

In summary, we have proposed and studied a novel spin filter which exploits quantum interference effects. The device comprises an FMI strip grown on top and/or below single-layer graphene. We showed that due to the exchange splitting induced by the magnetic ions of the FMI, the transmission coefficient is different for spin-up and spin-down electrons, giving rise to the polarization of the current density. By comparing different FMIs we found that those based on EuO/Gr/EuO heterostructures yield the highest efficiency. We conclude that the proposed device is a promising candidate for real world applications. In particular, it can be used as a tunable source of polarized electrons.

Acknowledgments

The authors thank A Díaz-Fernández for helpful discussions. This work has been supported by Ministerio de Ciencia e Innovación (Grants MAT2016-75955 and PID2019-106820RB-C21/2) and Junta de Castilla y León (Grants SA256P18 and SA121P20, including EU/FEDER funds).

Data availability statement

The data that support the findings of this study are available upon reasonable request from the authors.

ORCID iDs

C H Fuentevilla https://orcid.org/0000-0003-1969-3751
J D Lejarreta https://orcid.org/0000-0003-0301-0127
F Domínguez-Adame https://orcid.org/0000-0002-5256-4196
E Diez https://orcid.org/0000-0001-7964-4148

References

[1] Castro Neto A H, Guinea F, Peres N M R, Novoselov K S and Geim A K 2009 *Rev. Mod. Phys.* **81** 109
[2] Datta S and Das B 1990 *Appl. Phys. Lett.* **56** 665
[3] Jiang L and Zheng Y 2011 *J. Appl. Phys.* **109** 053701
[4] Huo Q H, Wang R Z and Yan H 2012 *Appl. Phys. Lett.* **101** 152404
[5] Lu W-T, Li W, Wang Y-L, Ye C-Z and Jiang H 2012 *J. Appl. Phys.* **112** 083712
[6] Yu X-X, Xie Y-E, Ou Y T and Chen Y-P 2012 *Chin. Phys.* B **21** 107202
[7] Faizabadi E, Esmaeilzadeh M and Sattari F 2012 *Eur. Phys. J.* B **85** 198
[8] Solis D, Hallal A, Waintal X and Chshiev M 2019 *Phys. Rev.* B **100** 104402
[9] Haugen H, Huertas-Hernando D and Brataas A 2008 *Phys. Rev.* B **77** 115406
[10] Swartz A G, Odenthal P M, Hao Y, Ruoff R S and Kawakami R K 2012 *ACS Nano* **6** 10063
[11] Savin H, Kuivalainen P, Lebedeva N and Novikov S 2014 *Phys. Status Solidi* B **251** 407
[12] Munárriz J, Domínguez-Adame F and Malyshev A V 2011 *Nanotechnology* **22** 365201
[13] Munárriz J, Domínguez-Adame F, Orellana P A and Malyshev A V 2012 *Nanotechnology* **23** 205202
[14] Saiz-Bretín M, Munárriz J, Malyshev A V and Domínguez-Adame F 2015 *Phys. Lett.* A **379** 2102
[15] Díaz E, Miralles K, Domínguez-Adame F and Gaul C 2014 *Appl. Phys. Lett.* **105** 103109
[16] Song Y and Dai G 2015 *Appl. Phys. Lett.* **106** 223104
[17] Song Y 2018 *J. Phys. D: Appl. Phys.* **51** 025002
[18] Yang H, Hallal A, Terrade D, Waintal X, Roche S and Chshiev M 2013 *Phys. Rev. Lett.* **110** 046603
[19] Hallal A, Ibrahim F, Yang H, Roche S and Chshiev M 2017 *2D Mater.* **4** 025074
[20] Su S, Barlas Y, Lee J, Shi J and Lake R 2017 *Phys. Rev.* B **95** 075418
[21] Tepper J and Barnaś J 2019 *J. Phys.: Condens. Matter* **31** 225302
[22] Büttiker M, Imry Y, Landauer R and Pinhas S 1985 *Phys. Rev.* B **31** 6207
[23] Datta S 1997 *Electronic Transport in Mesoscopic Systems* (Cambridge: Cambridge University Press)
[24] Ferry D and Goodnick S M 1999 *Transport in Nanostructures* (Cambridge: Cambridge University Press)
[25] Katsnelson M I, Novoselov K S and Geim A K 2006 *Nat. Phys.* **2** 620
[26] Lejarreta J D, Fuentevilla C H, Diez E and Cerveró J M 2013 *J. Phys. A: Math. Theor.* **46** 155304